RSC Advances

ROYAL SOCIETY OF CHEMISTRY

www.rsc.org/advances

Journal Name

ARTICLE

Large scale and facile sonochemical synthesis of magnetic graphene oxide nanocomposites and their dual electro/magneto-stimuli responses

Received 00th January 20xx,
Accepted 00th January 20xx

DOI: 10.1039/x0xx00000x

www.rsc.org/

Wen Ling Zhang,[a,c*] Yu Tian,[b] Ying Dan Liu,[c] Zhong Qian Song,[a] Jing Quan Liu,[a*] Hyoung Jin Choi[d*]

Graphene based magnetic nanoparticles (NPs) have attracted considerable attention in numerous applications owing to their splendid chemical and physical properties. However, the synthesis approaches are often complex and relatively expensive. In present work, we report a finding in fabricating magnetic graphene oxide (GO) nanocomposites (denoted as Fe_3O_4/GO) via an effective electrostatic strategy under ultrasonic waves, using the bare Fe_3O_4 NPs initially synthesized via co-precipitation method. The Fe_3O_4 NPs were covered uniformly by the crumple-like GO matrix as confirmed by Transmission electron microscope . Their structure and magnetic behaviors were investigated via Fourier transform infrared spectroscopy spectra and vibrating sample magnetometer curves. The appealing dual electro/magnetorheological performances of the as-prepared Fe_3O_4/GO dispersed in silicone oil were investigated using a rotational rheometer under applied electric or magnetic fields, respectively. Their dynamic yield stress values were analyzed using a universal equation, and the MR efficiency was observed to be higher than the ER one.

1. Introduction

An endeavor of discovery focused on graphene has created an entirely new branch of materials science and technology. Being a two-dimensional structure of carbon sheet, graphene owns high specific area, prominent electrical/thermal conductivity as well as excellent flexibility.[1-4] Benefiting from these interesting properties, graphene provides great potentials for a vast array of applications, including supercapacitors, batteries, fuel cells, sensors and actuators. Graphene oxide (GO) has been considered as one of the most desirable precursor to achieve mass production of graphene through exfoliation and reduction treatment. The surface bound oxygenous functional groups can be employed as active sites to render chemical modification or functionalization of GO sheets via covalent (chemical grafting) or noncovalent (π−π stacking, hydrogen bonding, electrostatic interactions) approaches.[5-7] On the other hand, the polar oxygenous functional groups will result in some loss in electrical conductivity. In recent years, extensive efforts have been made to attach magnetic nanoparticles (NPs) to GO or reduced GO (rGO) sheets by in-situ co-precipitation, physical affinities, microwave-heated synthesis, solvothermal route and even mechanochemical procedure.[8-12] Fe_3O_4 NPs have attracted intensive research due to their paramagnetic behaviors, cost-efficient and environmentally friendly properties.[13-17] However, their uncontrollable aggregation problems compromise their applications in nanotechnology and biomedical fields. To overcome these issues, considerable strategies have been developed. For instance, Zhong *et al.*[14] have reported 3D flower-like Fe_3O_4 NPs for water treatment. Fungus-like Fe_3O_4 NPs have also been fabricated for the removal of radionuclide.[18] The magnetic NPs have been decorated on layered double hydroxide (LDH) for drug release system.[19] Dai's group[20] have reported the in-situ fabrication of Fe_3O_4/rGO composites using Fe^{2+} as reducing agent. Besides, various other Fe_3O_4/GO composites have also been synthesized via metal-carbonyl coordination using functional solvent (1-methyl-2-pyrrolidone, NMP)[21] or electrostatic self-assembly approach.[22] In regards to other methods, electrostatic approach is considered as a suitable and economic choice to attach magnetic NPs on GO matrix. While the zeta potential of GO colloid is negative due to the surface-attached functional groups, simultaneously Fe_3O_4 NPs can be positively charged even in weak acidic solution. Therefore, it is possible to integrate magnetic particles on GO sheets via electrostatic attraction.[22,23] In present work, the pH of GO suspension was adjusted to 4 to create a favorable acidic environment for preparing positive charged Fe_3O_4 NPs.

Stimuli-responsive materials, which respond to external stimuli such as temperature, anion binding, pH, redox changes, mechanical force and electric or magnetic fields etc., especially

[a] College of Materials Science and Engineering, Laboratory of Fiber Materials and Modern Textile, Growing Base for State Key Laboratory, Qingdao University, Qingdao 266071, China.
[b] State Key Laboratory of Tribology, Tsinghua University, Beijing 100084, China.
[c] State Key Laboratory of Metastable Materials Science and Technology, Yanshan University, Qinhuangdao 066004, China.
[d] Department of Polymer Science and Engineering, Inha University, Incheon 402-751, Korea.
E-mail: wlzhangqd@qdu.edu.cn, jliu@qdu.edu.cn, hjchoi@inha.ac.kr

those with multiple responses, have recently attracted increasing attention to scientists and engineers.[24-29] In general, the ER suspensions are typically composed of polarizable particles within an insulating liquid, while the dispersed phase of MR fluids is magnetizable particles.[30-33] Under an applied electric or magnetic field, the particles will be polarized due to the dielectric constant mismatch between solid particles and medium oils. The dipole–dipole interaction among the polarized particles makes them align in the column-like structure, which changes their rheological properties (shear stress, shear viscosity, modulus etc.) dramatically.[34-37] These controllable characteristics of both ER and MR fluids have been developed in diverse engineering devices, such as clutches, engine mounts, brakes, dampers, valves, and even in bullet proof jackets.[38-41] In this paper, we reported the fabrication of Fe_3O_4/GO via electrostatic interaction and their dual electro/magneto-stimuli characteristics were critically discussed.

2. Experimental

2.1. Preparation of Fe_3O_4 nanoparticles

The magnetic Fe_3O_4 NPs were prepared using a chemical co-precipitation method.[9] $FeCl_3{\cdot}6H_2O$ and $FeCl_2{\cdot}4H_2O$ were dissolved in water under mechanical stirring under N_2 atmosphere. Aqueous ammonia was added quickly to precipitate Fe^{2+}/Fe^{3+} ions at 85 °C. After being rapidly stirred for 45 min, the black magnetic NPs were collected by a magnet, washed with water/ethanol, and lyophilized for 24 h.

2.2. Fabrication of Fe_3O_4/GO

GO sheets were synthesized by a modified Hummers' method[42] and washed until pH was 4. As shown in Scheme 1, the Fe_3O_4/GO was prepared following the procedure below: GO sheets were re-dispersed in water by sonication for 30 min, then the resultant Fe_3O_4 NPs were added. The mixture of GO and Fe_3O_4 (mass ratio of Fe_3O_4 and GO is 8:1) were stirred constantly under sonication by an ultrasonic generator (the operation power was 100 W and frequency was 40 kHz) for another 4 h. The product was collected via centrifugation and dried in an oven.

2.3 Synthesis of Fe_3O_4/GO based ER and MR fluids

The Fe_3O_4 NPs and Fe_3O_4/GO were dried in a vacuum oven at 60 °C for 24 h prior to the use. The electrical conductivity of Fe_3O_4/GO was about 10^{-7} S/cm which is in the suitable range for ER candidates (10^{-6}~10^{-10} S/cm). ER (15 wt%, particle concentration) and MR suspensions (20 vol%, particle concentration) were prepared by mixing the target Fe_3O_4/GO in silicone oil (100 cS, ρ=0.965). The suspensions were sonicated for 10 min before rheological measurements.

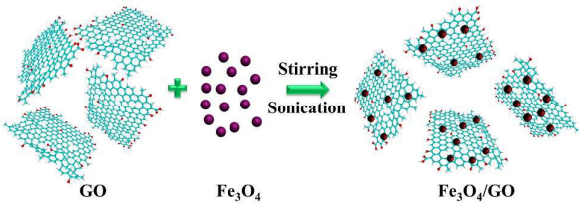

Scheme 1 Preparation procedure of Fe_3O_4/GO.

In general, the electro/magnetorheological (ER/MR) behaviors can be influenced by controlling the dispersed particle size, density, mass ratio and even their conductivities (especially for ER candidates). To achieve ideal ER/MR effects, ER fluid was prepared with 15 wt% particle concentration to avoid electric short during the ER measurement, while the MR fluid was prepared with 20 vol% particle concentration, aiming to achieve high magnetic field-induced yield stress.

2.4. Characterization

The morphology of the nanocomposite samples was examined by field emission transmission electron microscopy (FETEM, Tecnai G2 F20), while the chemical structures were measured by Fourier transform infrared spectroscopy (FT-IR, VERTEX 80v, Bruker). The resultant sample was pressed to a pellet and its electrical conductivity was measured using a four-probe type of resistivity meter (LORESTA-GP, MCP-T610). The magnetic characteristics were examined using a vibrating sample magnetometer (VSM, Lake Shore 7307). X-ray photoelectron spectroscopy (XPS) signals were acquired on a Thermo Escalab 250XI spectrometer. Raman spectra were measured using a Renishaw RM2000 Raman system. The thermal stability was studied using a thermalgravimetric analyzer (TGA, TA Q50, heating rate 10 °C/min) in the N_2 environment. Inductive coupled plasma emission spectrometer (ICP-MS, Agilent 7500ce) was applied to study the accurate composition of the sample. As for main topics in this study, the ER behaviors were examined using a rotational rheometer (Physica MCR300, Anton Paar) equipped with a high-voltage generator using a Couette-type cylinder geometry (CC 17, gap distance is 0.71 mm), while the same type rheometer equipped with a MR device (Physica MRD180) using a parallel-plate cell (PP 20, gap distance is 1mm) was employed for the MR measurements. The ultrasonic generator (KQ-100DE, Kunshan Ultrasonic Instruments Co., Ltd) was used during the sonication process.

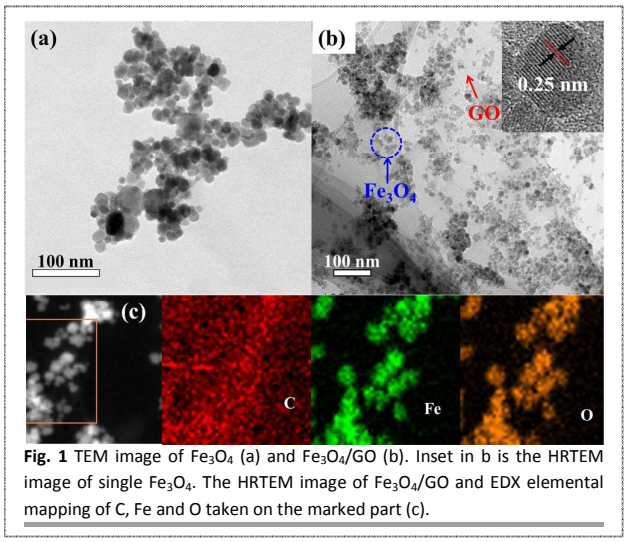

Fig. 1 TEM image of Fe_3O_4 (a) and Fe_3O_4/GO (b). Inset in b is the HRTEM image of single Fe_3O_4. The HRTEM image of Fe_3O_4/GO and EDX elemental mapping of C, Fe and O taken on the marked part (c).

Results and discussion

The morphologies of bare Fe_3O_4 NPs and Fe_3O_4/GO were measured by TEM images. As shown in Fig. 1a, the Fe_3O_4 NPs were aggregated seriously with an average single particle diameter of ca. 10 nm. In the case of Fe_3O_4/GO (Fig. 1b), Fe_3O_4 nanoparticles were observed to be uniformly distributed on the crumple-like GO sheets. As shown in the inset of Fig. 1b, the adjacent lattice spacing of Fe_3O_4 was 0.25 nm, which was assigned to the (311) plane.[43] The EDX elemental mapping of Fe_3O_4/GO (Fig. 3c) indicated that the Fe and O elements were homogeneously distributed on C element, confirming that the GO sheets were decorated by Fe_3O_4 nanoparticles. The attachment of Fe_3O_4 on GO sheets can avoid the re-stacking of GO and aggregation of Fe_3O_4 NPs, leading to good dispersion stability for preparing the ER/MR fluids.

In order to verify the combination of Fe_3O_4 with GO, FT-IR spectra of bare Fe_3O_4 NPs, Fe_3O_4/GO and GO sheets were collected. As shown in Fig. 2a, the bands of hydroxyl was observed at 3440 cm^{-1}, along with epoxy (1228 cm^{-1}) and carbonyl (1730 cm^{-1}) groups associated with GO sheets.[44] In Fe_3O_4 spectrum, the strong peak at 584 cm^{-1} should be corresponded to the stretching vibration of Fe–O bond.[45] In the spectrum of Fe_3O_4/GO, the peaks for GO sheets at 1234 cm^{-1} and 1732cm^{-1} corresponding to the epoxy and carbonyl groups were observed. An obvious peak at about 586cm^{-1} can be attributed to the Fe–O bond, evidencing the presence of Fe_3O_4 NPs.

The magnetic hysteresis curves of bare Fe_3O_4 NPs and Fe_3O_4/GO at room temperature were recorded as shown in Fig. 2b. It can be seen that both of the samples exhibited paramagnetic behaviors, which is suitable for MR applications. The saturation magnetization (M_s) of Fe_3O_4/GO (52.2 emu/g) decreased by 9.2 emu/g compared to that of bare Fe_3O_4 NPs (61.4 emu/g) due to the presence of weak or non-magnetic GO sheets. If we ignore the magnetic behavior of GO, the mass ratio of Fe_3O_4 NPs in the Fe_3O_4/GO calculated from VSM curve was 85 wt%, which is close to the feed ratio for the experiment (~88.89 wt%).

The concentration of Fe was accurately measured using ICP-MS, and the value was 59.72wt%, which was a little lower compared to the value calculated from the experimental ratio (Fe~64.36 wt%). And then, the mass ratio between Fe_3O_4 and GO (~5:1) in Fe_3O_4/GO from the ICP-MS measurement was calculated. A deviation from the experimental ratio (~8:1) and ICP-MS measurement (~5:1) was observed, which may due to the unavoidable experimental errors.

The elemental composition of the as-prepared samples was analysed by X-ray diffraction (XRD) pattern. As shown in Fig. 2c the XRD patterns of both the bare Fe_3O_4 NPs and Fe_3O_4/GO exhibited the intense diffraction peaks indexed to (220), (311), (400), (422), (511), and (440) planes appeared at 2θ = 30.20°, 35.76°, 43.40°, 53.75°, 57.31° and 62.89°, respectively, which were consistent with the standard XRD data for face-centered cubic crystals of Fe_3O_4 (JCPDS 19-0629).[46,47] The broad diffraction peaks indicated that the size of Fe_3O_4 NPs was small. The peak at 10.64° was a characteristic peak of GO.[48,49] It is difficult to find the typical peak of GO in Fe_3O_4/GO maybe because of its low content. To confirm our conjecture, the Fe_3O_4/GO with higher mass ratio of GO to Fe_3O_4 (GO:Fe_3O_4 = 1:2) were prepared and the XRD pattern was measured. As shown in the inset of Fig. 2c, the GO peak can be clearly detected.

Thermal stabilities of the samples were determined by a thermogravimetric analyzer (TGA) in nitrogen atmosphere (Fig. 2d). The initial weight loss for GO below 150 °C was associated with the evaporation of water molecules physically adsorbed onto the hydrophilic GO surface. The remaining of Fe_3O_4/GO was about 85.4 wt%, which is higher than that of bare GO sheets (41.42 wt%), confirming the enhanced thermal stability of the loaded Fe_3O_4 NPs.

Based on the fact that Raman spectra provide a reliable evidence to characterize the structural changes of carbonaceous materials, Fig. 3a shows the Raman spectra of GO and Fe_3O_4/GO. Two prominent peaks of GO located at 1600 and 1357 cm^{-1} were

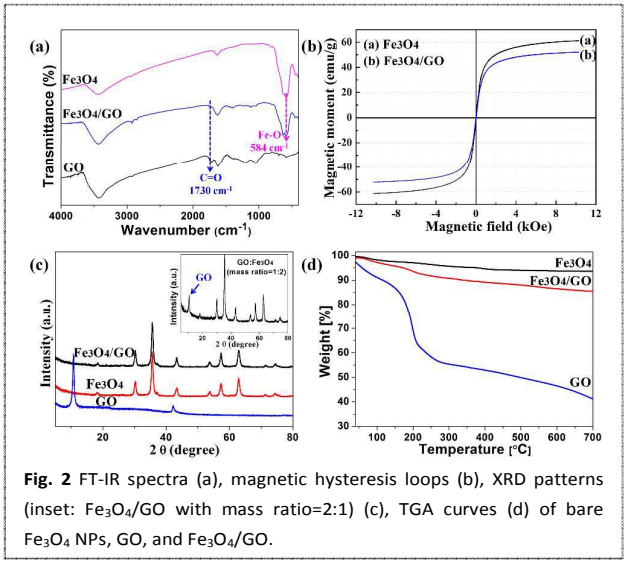

Fig. 2 FT-IR spectra (a), magnetic hysteresis loops (b), XRD patterns (inset: Fe_3O_4/GO with mass ratio=2:1) (c), TGA curves (d) of bare Fe_3O_4 NPs, GO, and Fe_3O_4/GO.

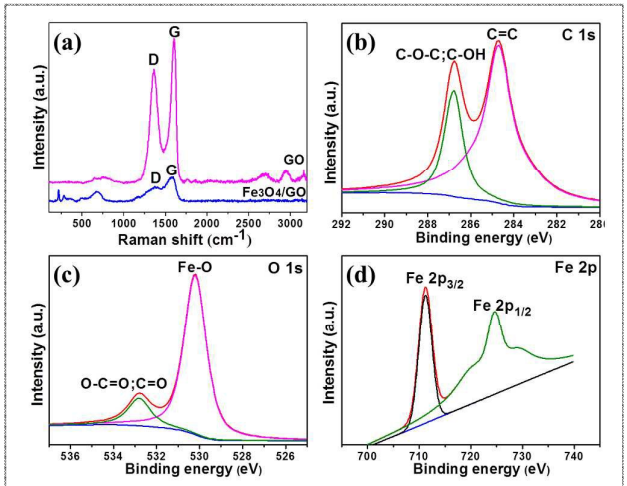

Fig. 3 Raman spectra of GO and Fe_3O_4/GO (a), XPS spectra scans of C 1s (b), O 1s (c) and Fe 2p (d) of Fe_3O_4/GO.

observed, corresponding to the G and D bands, respectively. Generally, the G band is attributed to the first-order scattering of C sp^2 atom domains of graphite, and the D band ascribed to the vibration of sp^3-hybridized carbon bonds of the disordered GO.[50] From the Raman spectrum of Fe_3O_4/GO, typical peaks of GO at 1580 and 1355 cm^{-1} were also observed, confirming the presence of GO. The intensity ratio of D and G bands (I_D/I_G) can be utilized to study the graphitization degree and the defect density of the carbonaceous materials. The Fe_3O_4/GO exhibited a decreased value of I_D/I_G (0.62) in comparison with that of the bare GO (~0.78), implying that the decoration of Fe_3O_4 on GO layers did not introduce more defects into the Fe_3O_4/GO.

The XPS pattern of Fe_3O_4/GO is shown in Fig. 3b-d. From the C1s spectrum (Fig. 3b), the peak located at 286.7 eV was assigned to the C-OH or C-O-C, while the peak at 284.6 eV was attributed to characteristic peak of C=C sp^2. The O 1s spectrum of Fe_3O_4/GO (Fig. 3c) exhibited a sharp peak at 530.2 eV, which was ascribed to the lattice oxygen of Fe_3O_4 (Fe-O). The peak at 532.8 eV was assigned to the oxygen in carbonyl or carboxylate (O-C=O; C=O). For the high-resolution XPS spectrum of Fe 2p scan (Fig. 3d), the binding energy peaks at 711.2 and 724.7 eV were corresponding to Fe $2p_{3/2}$ and Fe $2p_{1/2}$, respectively. There is no charge transfer satellite around 720 eV for γ–Fe_2O_3, revealing the only existence of Fe_3O_4 in Fe_3O_4/GO. [51]

The Fe_3O_4/GO based ER fluid was measured using a rotational rheometer. As described in Fig. 4a, the shear stress increased linearly with the increased shear rate under free electric field, indicating a typical Newtonian behavior. When an external electric field stress was applied, yield stress appeared. The shear stress was enhanced with the increasing external electric fields, confirming the formation of robust fibril-like structure in response to external electric stimulus. From Fig. 4b, the viscosity of the Fe_3O_4/GO based ER fluid was derived to be 0.14 Pa·s. Typical shear-thinning behaviors were observed under an applied electric field.

Dynamic oscillation tests of the Fe_3O_4/GO based ER fluid were conducted to characterize its viscoelastic properties. As shown in Fig. 4c,d the storage modulus (G') was observed to be

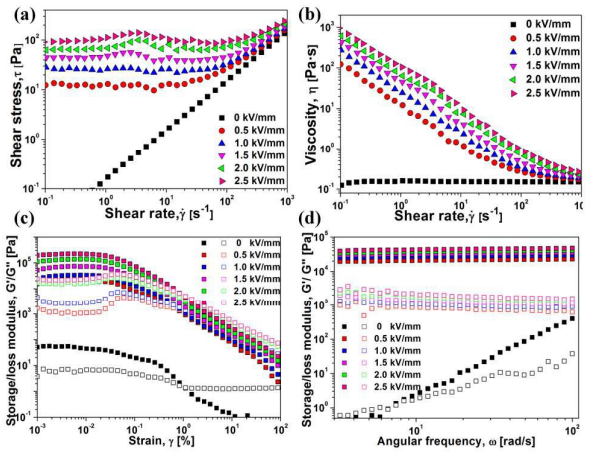

Fig. 4 Rotational measurements: Shear stress (a) and shear viscosity (b) vs. shear rate; Oscillation measurements: Amplitude (c) and frequency (d) for Fe_3O_4/GO based ER fluid (γ=0.004%).

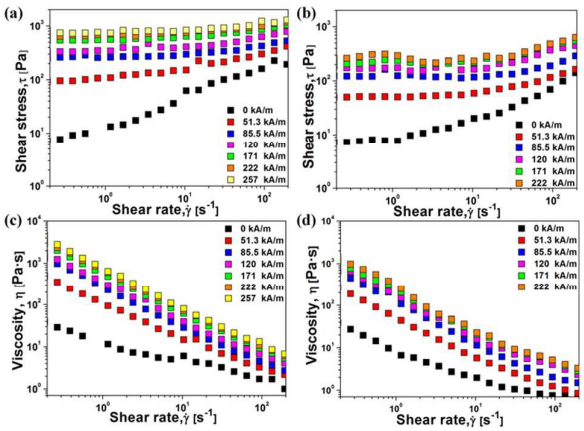

Fig. 5 The shear stress and viscosity vs. shear rate for bare Fe_3O_4 NPs (a, c) and Fe_3O_4/GO (b, d) based MR fluid.

larger than the loss modulus (G''), and these values were independent of the frequency within the regions of strain applied (0.004%) under different electric field (Fig. 4c). From the frequency sweep (Fig. 4d), the increase of G' with the applied electric field indicated that the ER fluid became more elastic under its linear viscoelastic conditions. In addition, the G' and G'' increased linearly with the increasing frequency under free electric field, indicating a fluid-like state.

The flow curves of bare Fe_3O_4 NPs and Fe_3O_4/GO based MR fluids were investigated and compared. As shown in Fig. 5, similar shear stress tendency of these two MR fluids was observed with and without the application of external magnetic fields, proving their characteristic MR performances. The bare Fe_3O_4 NPs based MR fluids reached saturation at 257 kA/m (Fig. 5a,c) while Fe_3O_4/GO based MR fluid reached saturation at 222 kA/m due to the weakened magnetic properties resulting from the presence of GO sheets (Fig. 5b,d).

The yield stress τ_y, which associates with electric/magnetic field strength (E/H), particle volume fraction ϕ and other parameters, is an important factor to evaluate the ER or MR effects. A correlation between the dynamic yield stress and electric field strength of Fe_3O_4/GO based ER fluid is represented in Fig. 6a. The slope was derived to be 1.5, revealing a conduction model.[52,53]

Similar to ER fluids,[54] a universal yield stress equation (Eq. 1) was proposed to correlate the relationship between dynamic yield stress (τ_y) and magnetic field strengths (H_0) for MR fluids.[55]

$$\tau_y(H_0) = \alpha H_0^2 \left(\frac{tanh\sqrt{H_0/H_c}}{\sqrt{H_0/H_c}} \right) \qquad (1)$$

where, α depends on the volume fraction and other analogous physical parameters of the MR fluids. τ_y possesses two regimes with respect to H_0:

$$\tau_y = \alpha H_0^2 \text{for} H_0 \ll H_c \qquad (2.1)$$

$$\tau_y = \alpha \sqrt{H_c} H_0^{3/2} \text{for} H_0 \gg H_c \qquad (2.2)$$

As for the analysis of bare Fe_3O_4 NPs and Fe_3O_4/GO based MR fluids, their dynamic yield stresses were collected. As shown in Fig. 6b the slope decreased from 2 (at low magnetic field strength) to 1.5 (at high magnetic field strength). A critical magnetic field strength (H_c) was obtained to be 171 kA/m from the crossover point of the slope.

In order to illustrate the data using a single curve, a generalized scaling expression was proposed by normalizing Eq. 1 using H_c and $\tau_y(H_c)=0.762\alpha H_c^2$:

$$\hat{\tau} = 1.313\hat{H}^{3/2}\tanh\sqrt{\hat{H}} \qquad (3)$$

$$\text{where, } \hat{H} \equiv H_0/H_c \text{and} \hat{\tau} \equiv \tau_y(H_0)/\tau_y(H_c)$$

The data obtained from Fig. 6b were fit via Eq. 3 to derive a single curve as shown in Fig. 6c. However, the points $(\hat{\tau}, \hat{H})$ deviated from the curves of Eq. 3. To fit these data more precisely, one additional parameter b was employed and Eq. 3 was then modified as following:

$$\hat{\tau} = 1.313\hat{\hat{H}}^{3/2}\tanh\sqrt{\hat{\hat{H}}} \qquad (4)$$

$$\hat{\hat{H}} \equiv \hat{H}^{1+2b} \text{and} \hat{\tau} \equiv \hat{\tau}\hat{H}^{4b}$$

Fig. 6d shows the universal fitting using Eq. 4 with b = 0.56, all the points $(\hat{\hat{\tau}}, \hat{\hat{H}})$ showed excellent agreement with the universal line.

Besides yield stress, ER or MR efficiency is another parameter for evaluating the electro/magneto responsive performances under electric or magnetic stimuli. The ER or MR efficiency can be defined as $I = (\tau_{E/M}-\tau_0)/\tau_0$ or $I = (\eta_{E/M} - \eta_0)/\eta_0$, where $\tau_{E/M}$ or $\eta_{E/M}$ is the shear stress or shear viscosity with an electric/magnetic field and τ_0 or η_0 is the shear stress or shear viscosity without an electric/magnetic field, respectively.[31] In Fig. 7, ER and MR efficiencies of Fe_3O_4/GO based suspensions are plotted as a function of shear rate. It can be seen that the ER or MR efficiency decreased sharply with the increasing shear rate, which attributes to the progressively destroyed gap-spanning particle chains. In addition, the MR efficiency was lower than that of the ER one, which should be due to its high free-field shear stress (τ_0) originated from the high particle concentrations.

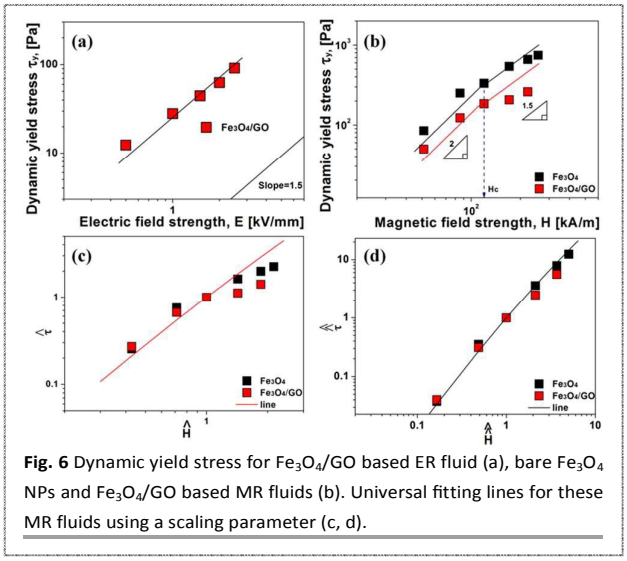

Fig. 6 Dynamic yield stress for Fe_3O_4/GO based ER fluid (a), bare Fe_3O_4 NPs and Fe_3O_4/GO based MR fluids (b). Universal fitting lines for these MR fluids using a scaling parameter (c, d).

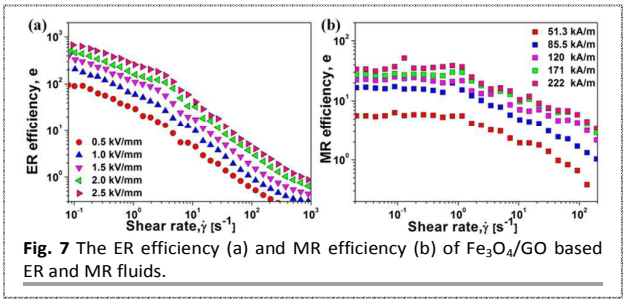

Fig. 7 The ER efficiency (a) and MR efficiency (b) of Fe_3O_4/GO based ER and MR fluids.

Conclusions

Magnetic GO nanocomposites (Fe_3O_4/GO) were successfully synthesized via an effective electrostatic attraction strategy. The loading of Fe_3O_4 nanoparticles on GO surface effectively avoids the re-stacking process of GO sheets. The excellent dual electro/magneto-responsive behaviors of the as-prepared Fe_3O_4/GO based suspensions were achieved, which can be ascribed to the paramagnetic properties of Fe_3O_4 and polarization properties of GO sheets. Our future research will focus on the rheological behaviors of Fe_3O_4/GO based suspensions under electric and magnetic fields simultaneously. It will be a great challenge in mechanical control fields.

Acknowledgements

This work was supported by Qingdao Innovation Leading Expert Program, Qingdao Basic & Applied Research project (15-9-1-100-jch), National Natural Science Foundation of China (Grant No. 51323006), the Open Fund of State Key Laboratory of Metastable Materials Science and Technology (Yanshan University, 201608) and the Tribology Science Fund of State Key Laboratory of Tribology (SKLTKF15A10).HJ Choi was partially supported by National Research Foundation, Korea (2016R1A2B4008438)

Notes and references

1 S. Bi, M. Chen, X. Jia and Y. Dong, *Nanoscale*, 2015, **7**, 3745.
2 M. D. Stoller, S. J. Park, Y. W. Zhu, J. H. An and R. S. Ruoff, *Nano Lett.*, 2008, **8**, 3498.
3 X. Huang, X. Qi, F. Boey and H. Zhang, *Chem. Soc. Rev.*, 2012, **41**, 666.
4 Y. C. Fan, W. Jiang and A. Kawasaki, *Adv. Funct. Mater.*, 2012, **22**, 3882-3889.
5 P. Kumar, H. P. Mungse, S. Cordier, R. Boukherroub, O. P. Khatri and S. L. Jain, *Carbon*, 2015, **94**, 91.
6 D. R. Dreyer, S. Park, C. W. Bielawski and R. S. Ruoff, *Chem. Soc. Rev.*, 2010, **39**, 228.
7 L. Zhang, J. Xia, Q. Zhao, L. Liu and Z. Zhang, *Small*, 2010, **6**, 537.
8 T. Jiao, Y. Liu, Y. Wu, Q. Zhang, X. Yan, F. Gao, A. J. P. Bauer, J. Liu, T. Zeng and B. Li, *Sci. Rep.*, 2015, **5**, 12451.
9 X. Y. Yang, X. Y. Zhang, Y. F. Ma, Y. Huang, Y. S. Wang and Y. S. Chen,*J. Mater. Chem.*, 2009, **19**, 2710-2714.

10 X. J. Fan, G. Z. Jiao, W. Zhao, P. F. Jin and X. Li, *Nanoscale*, 2013, **5**, 1143.
11 G. Cheng, Y.-L. Liu, Z.-G. Wang, J.-L. Zhang, D.-H. Sun and J.-Z. Ni,*J. Mater. Chem.*, 2012, **22**, 21998.
12 B. Karagoz, J. Yeow, L. Esser, S. M. Prakash, R. P. Kuchel, T. P. Davis and C. Boyer, *Langmuir*, 2014, **30**, 10493.
13 S. H. Sun and H. Zeng, *J. Am. Chem. Soc.*, 2002, **124**, 8204.
14 L. S. Zhong, J. S. Hu, H. P. Liang, A. M. Cao, W. G. Song and L. J. Wan, *Adv. Mater.*, 2006, **18**, 2426.
15 M. Mahmoudi, S. Sant, B. Wang, S. Laurent and T. Sen, *Adv. Drug Delivery Rev.,* 2011, **63**, 24.
16 A. Perez del Pino, E. Gyoergy, C. Logofatu, J. Puigmarti-Luis and W. Gao, *Carbon*, 2015, **93**, 373.
17 C. Ding, W. Cheng, Y. Sun and X. Wang, *J. Hazard. Mater.*, 2015, **295**, 127.
18 F. Lv, L. Xu, Y. Zhang and Z. Meng, *ACS Appl. Mater. Interfaces*, 2015, **7**, 19104.
19 S. K. Sahu, B. Huang, K. Lilova, B. F. Woodfield and A. Navrotsky, *Phys. Chem. Chem. Phys.*, 2015, **17**, 22286.
20 Y. H. Xue, H. Chen, D. S. Yu, S. Y. Wang, M. Yardeni, Q. B. Dai, M. M. Guo, Y. Liu, F. Lu, J. Qu and L. M. Dai, *Chem. Commun.*, 2011, **47**, 11689.
21 J. F. Shen, Y. Z. Hu, M. Shi, N. Li, H. W. Ma and M. X. Ye, *J. Phys. Chem. C*, 2010, **114**, 1498.
22 Q. Han, Z. H. Wang, J. F. Xia, S. Chen, X. Q. Zhang and M. Y. Ding, *Talanta*, 2012, **101**, 388.
23 X. Han, L. G. Gai, H. H. Jiang, L. C. Zhao, H. Liu and W. Zhang, *Synth. Met.*, 2013, **171**, 1.
24 M. Cabuk, M. Yavuz and H. I. Unal, *J. Intell. Mater. Syst. Struct.*, 2015, **26**, 1799-1810.
25 P. Chen and N. Holten-Andersen, *Adv. Opt. Mater.*, 2015, **3**, 1041-1046.
26 Ubaidillah, J. Sutrisno, A. Purwanto and S. A. Mazlan, *Adv. Eng. Mater.*, 2015, **17**, 563.
27 V. A. Pletneva, V. S. Molchanov and O. E. Philippova, *Langmuir*, 2015, **31**, 110.
28 H. Wang, B. Tan, H. Zhang and J. Wang, *RSC Adv.*, 2015, **5**, 65583.
29 C.-M. Yoon, K. Lee, J. Noh, S. Lee and J. Jang, *J. Mater. Chem. C*, 2016, **4**, 1713.
30 J. L. Jiang, Y. Tian and Y. G. Meng, *Langmuir*, 2011, **27**, 5814.
31 J. Yin, Y. Shui, Y. Dong and X. Zhao, *Nanotechnology*, 2014, **25**, 045702.
32 C. Guo, X. Gong, S. Xuan, Q. Yan and X. Ruan, *Smart Mater. Struct.*, 2013, **22**, 045020.
33 W. J. Wen, X. X. Huang, S. H. Yang, K. Q. Lu and P. Sheng, *Nat. Mater.*, 2003, **2**, 727.
34 34. D. E. Park, H. S. Chae, H. J. Choi and A. Maity, *J. Mater. Chem. C*, 2015, **3**, 3150.
35 T. Plachy, M. Mrlik, Z. Kozakova, P. Suly, M. Sedlacik, V. Pavlinek and I. Kuritka, *ACS Appl. Mater. Interfaces*, 2015, **7**, 3725.
36 S. H. Kim, J. H. Kim, H. J. Choi and J. Park, *RSC Adv.*, 2015, **5**, 72387.
37 X. Dong, N. Ma, H. Yang, B. Han and M. Qi, *RSC Adv.*, 2015, **5**, 74656.
38 S. Ryu, J.-H. Koo, T.-H. Yang, D. Pyo, K.-U. Kyung and D.-S. Kwon, *J. Intell. Mater. Syst. Struct.*, 2015, **26**, 1670.
39 G. Hu, Y. Ru and W. Li, *J. Intell. Mater. Syst. Struct.*, 2015, **2**6, 527-540.
40 W. L. Zhang, J. Liu and H. J. Choi, *J.Nanomater.*, 2015, **2015**, 574637.
41 J. S. Oh, S. H. Choi and S. B. Choi, *Smart Mater. Struct.*, 2014, **23**, 095032.
42 B. Neppolian, C. Wang and M. Ashokkumar, *Ultrason. Sonochem.*, 2014, **21**, 1948.
43 F. Gu, M. Liang, D. Han and Z. Wang, *RSC Advances*, 2015, **5**, 39964.
44 Y. Wang, D. Zhang, Q. Bao, J. Wu and Y. Wan, *J. Mater. Chem.*, 2012, **22**, 23106.
45 F. Zhang, Y. Song, S. Song, R. Zhang and W. Hou, *ACS Appl. Mater. Interfaces*, 2015, **7**, 7251.
46 M. Liu, C. Chen, J. Hu, X. Wu and X. Wang, *J. Phys. Chem. C*, 2011, **115**, 25234.
47 X. Xu, H. Li, Q. Zhang, H. Hu, Z. Zhao, J. Li, J. Li, Y. Qiao and Y. Gogotsi, *ACS Nano*, 2015, **9**, 3969.
48 D. C. Marcano, D. V. Kosynkin, J. M. Berlin, A. Sinitskii, Z. Z. Sun, A. Slesarev, L. B. Alemany, W. Lu and J. M. Tour, *ACS Nano*, 2010, **4**, 4806.
49 Z. Bo, X. Shuai, S. Mao, H. Yang, J. Qian, J. Chen, J. Yan and K. Cen, *Sci. Rep.*, 2014, **4**, 4684.
50 Y. Shao, T. Jing, J. Tian and Y. Zheng, *RSC Adv.,* 2015, **5**, 103943.
51 B. Yang, J. Zhao, J. Chen, M. He and S. Xu, *RSC Adv.*, 2015, **5**, 57906.
52 M. Sedlacik, M. Mrlik, V. Pavlinek, P. Saha and O. Quadrat, *Colloid. Polym. Sci.*, 2012, **290**, 41.
53 W. L. Zhang and H. J. Choi, *Soft Matter*, 2014, **10**, 6601.
54 H. J. Choi, M. S. Cho, J. W. Kim, C. A. Kim and M. S. Jhon, *Appl. Phys. Lett.*, 2001, **78**, 3806.
55 F. F. Fang, H. J. Choi and M. S. Jhon, *Colloids and Surfaces A: Physicochem. Eng. Aspects*, 2009, **351**, 46.

Large scale and facile sonochemical synthesis of magnetic graphene oxide nanocomposites and their dual electro/magneto-stimuli responses

Wen Ling Zhang,[a,c*] Yu Tian,[b] Ying Dan Liu,[c] Zhong Qian Song,[a] Jing Quan Liu,[a*] Hyoung Jin Choi[d*]

[a.] College of Materials Science and Engineering, Laboratory of Fiber Materials and Modern Textile, Growing Base for State Key Laboratory, Qingdao University, Qingdao 266071, China.

[b.] State Key Laboratory of Tribology, Tsinghua University, Beijing 100084, China.

[c.] State Key Laboratory of Metastable Materials Science and Technology, Yanshan University, Qinhuangdao 066004, China.

[d.] Department of Polymer Science and Engineering, Inha University, Incheon 402-751, Korea.

E-mail: wlzhangqd@qdu.edu.cn, jliu@qdu.edu.cn, hjchoi@inha.ac.kr

Magnetic Fe_3O_4/GO nanocomposites have been prepared via an effective electrostatic strategy under ultrasonic waves. Their appealing dual electro/magnetorheological (ER/MR) performances were investigated under applied electric or magnetic fields, respectively.